AD-A183 343 INVESTIGATIONS AT THE N-HFS2/NON-AQUEOUS ELECTROLYTE INTERFACIAL REGION(U) ELTRON RESEARCH INC AURORA IL K W SEMKOW ET AL. JUL 87 N00014-86-C-0128 1/1

UNCLASSIFIED F/G 7/2 NL

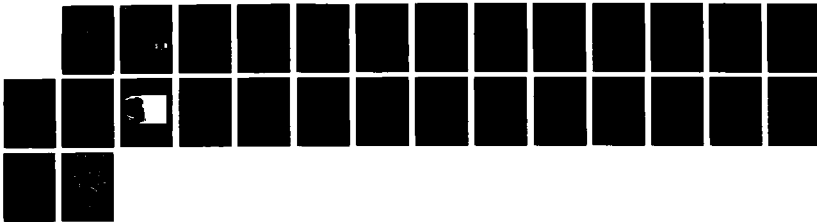

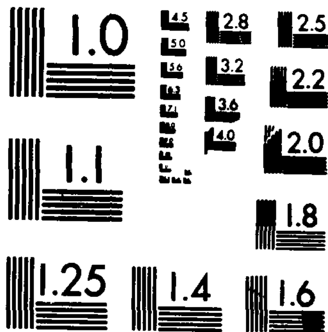

MICROCOPY RESOLUTION TEST CHART
NATIONAL BUREAU OF STANDARDS-1963-A

DTIC FILE COPY

(12)

SECURITY CLASSIFICATION OF THIS PAGE (When Data Entered)

REPORT DOCUMENTATION PAGE

READ INSTRUCTIONS BEFORE COMPLETING FORM

1. REPORT NUMBER: 2
2. GOVT ACCESSION NO.:
3. RECIPIENT'S CATALOG NUMBER:

4. TITLE (and Subtitle): Investigations at the n-HfS_2/Non-Aqueous Electrolyte Interfacial Region

5. TYPE OF REPORT & PERIOD COVERED: Technical, Oct. 1986 - July 1987

6. PERFORMING ORG. REPORT NUMBER:

7. AUTHOR(s): K. W. Semkow, N. U. Pujare and A. F. Sammells

8. CONTRACT OR GRANT NUMBER(s): N00014-86-C-0128

9. PERFORMING ORGANIZATION NAME AND ADDRESS: Eltron Research, Inc., 4260 Westbrook Drive, Aurora, IL 60504

10. PROGRAM ELEMENT, PROJECT, TASK AREA & WORK UNIT NUMBERS:

11. CONTROLLING OFFICE NAME AND ADDRESS: Office of Naval Research/Chemistry Program, Arlington, VA 22217

12. REPORT DATE: July 1987

13. NUMBER OF PAGES: 26

14. MONITORING AGENCY NAME & ADDRESS (if different from Controlling Office): Above

15. SECURITY CLASS. (of this report): Unclassified

15a. DECLASSIFICATION/DOWNGRADING SCHEDULE:

16. DISTRIBUTION STATEMENT (of this Report)

Approved for public release, distribution unlimited.

DTIC ELECTE AUG 05 1987 S D

17. DISTRIBUTION STATEMENT (of the abstract entered in Block 20, if different from Report)

Approved for public release, distribution unlimited.

18. SUPPLEMENTARY NOTES

Submitted: Journal of the Electrochemical Society

19. KEY WORDS (Continue on reverse side if necessary and identify by block number)

Hafnium disulfide, admittance spectroscopy, van der Waals surfaces, photoelectrodes.

AD-A183 343

20. ABSTRACT (Continue on reverse side if necessary and identify by block number)

Single crystal n-HfS_2 photoelectrodes prepared by halogen vapor transport were investigated in 0.1M $TBAPF_6/CH_3CN$ electrolyte using both impedance and admittance spectroscopy techniques. The presence of frequency dependent capacitive and resistive elements in the equivalent circuit for n-HfS_2/electrolyte interface were evident. Measured capacitance effects at the interfacial region were found dependent upon the crystal orientation used, with that for defect free van der Waals surfaces being $10^{-8}F/cm^2$; an order of magnitude lower than for n-HfS_2 intercalation layers exposed to the electrolyte. High capacitance values were correlated with a high population

DD FORM 1473 EDITION OF 1 NOV 65 IS OBSOLETE

87 8 4 037

Unclassified

SECURITY CLASSIFICATION OF THIS PAGE (When Data Entered)

INVESTIGATIONS AT THE n-HfS_2/NON-AQUEOUS ELECTROLYTE INTERFACIAL REGION

Krystyna W. Semkow*, Nirupama U. Pujare and Anthony F. Sammells*

Eltron Research, Inc.
Aurora, Illinois 60504

ABSTRACT

Single crystal n-HfS_2 photoelectrodes prepared by halogen vapor transport were investigated in 0.1M $TBAPF_6/CH_3CN$ electrolyte using both impedance and admittance spectroscopy techniques. The presence of frequency dependent capacitive and resistive elements in the equivalent circuit for n-HfS_2/electrolyte interface were evident. Measured capacitance effects at the interfacial region were found dependent upon the crystal orientation used, with that for defect free van der Waals surfaces being $10^{-8}F/cm^2$; an order of magnitude lower than for n-HfS_2 intercalation layers exposed to the electrolyte. High capacitance values were correlated with a high population of surface charges. Admittance spectroscopy analysis suggested the presence of surface states associated with surface adsorption processes. Open-circuit photovoltages up to 0.35V under $100mW/cm^2$ illumination were observed for van der Waals surfaces, decreasing to 0.16V as the population intercalating layers exposed to the electrolyte was increased.

Accesion For
NTIS CRA&I
DTIC TAB
Unannounced
Justification
By
Distribution /
Availability Codes
Dist
A-1

*Electrochemical Society Active Member

Key Words: hafnium disulfide, interfacial capacitance, non-aqueous electrolyte

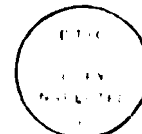

Considerable work has already been reported[1-10], directed towards investigating the photoelectrochemical (PEC) properties of transition metal dichalcogenides (TMDs) belonging to the periodic groups IV, VI and VIII. These materials all possess a layer type structure between the transition metal and chalcogenide, held together by relatively weak van der Waals forces. The electronic structure of these materials and corresponding PEC characteristics are dependent in part, upon whether the dichalcogenide possesses an octahedral or trigonal prismatic type structure.

For group IVB TMDs (HfS_2, $HfSe_2$, ZrS_2 and $ZrSe_2$) which possess an octahedral structure, electron photoexcitation within the semiconductor band gap proceeds from energy bands derived from bonding sulfur p-orbitals into metal d-orbitals (t_{2g})[11-18]. By comparison group VIB TMDs (MoS_2, WSe_2) possess a trigonal prismatic symmetry which result in a splitting of the t_{2g} d-orbitals into lower (d_{z^2}) and upper (d_{xy} and $d_{x^2-y^2}$) states. In this latter case photoelectron excitation will occur between these TMD split non-bonding d-orbitals[2,11,12]. All of these semiconductors possess indirect band gaps, although their absorption coefficients are quite high, with most photons becoming captured within 1000Å from the interfacial region[12]. Group VIB based photoelectrodes have previously been investigated by us in both regenerative[19] and ex situ storage PEC cells[20] where they have demonstrated good stability against photoanodic corrosion.

One alternative strategy for the storage of incident PEC energy would be to exploit the reversible intercalation of redox metal species within layer type photoelectrodes themselves. In the case of molybdenum and tungsten dichalcogenides their van der Waal layers are incompatible for the reversible intercalation of reduced transition metal species. Group IVB dichalcogenides by comparison have the potential ability to function both as photoelectrodes and as the substrate electrode for subsequent reversible intercalation of reduced transition metal species[11,21-28]. It has already been reported[24] that p-ZrS_2 is capable of maintaining its semiconducting properties after partial intercalation by either Cu or Fe to form ZrM_yS_2 while the degree of intercalation will vary as, $0 < y < 0.22$, although these photoelectrodes will become progressively more degenerate during intercalation, due to an increasing conduction band population.

We have recently become interested in the group IVB TMDs, with particular emphasis being placed upon n-HfS_2 (band gap 1.96eV) because of the encouraging

photopotential observed by us from this material (up to -350mV in acetonitrile based electrolytes). This has resulted in the preparation and the on going investigation of solid-state two photoelectrode storage PEC cells possessing the general configuration:

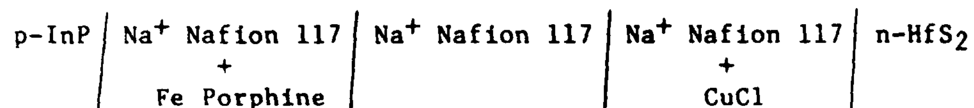

The van der Waals layers available in single crystal n-HfS_2 for the intercalation of metal species resident in close proximity to the interfacial region during electrochemical discharge of the above cell, are shown in Figure 1. During electrochemical discharge interfacial Cu^+ species become reduced followed by their subsequent intercalation within the n-HfS_2 van der Waals layer. PEC charge of the photoanode interfacial region will occur via the promotion of photoexcited electron holes from the n-HfS_2 valence band leading to the photodeintercalation of copper and formation of cuprous ions. The performance that might be realized from such solid-state PEC storage devices will be determined in part by the population of exposed van der Waals layers resident at the interfacial region. Too high a population of exposed intercalation layers will inhibit PEC performance via recombination of photogenerated carriers, whereas too low a population will limit the Faradaic capacity of this intercalating photoelectrode.

As a consequence of the above discussion it is evident that there is a clear incentive to perform some characterization of the n-HfS_2/electrolyte interfacial region as a function of crystal orientation. This has been addressed here by the application of impedance and admittance techniques to investigate the n-HfS_2/electrolyte interfacial region initially in the absence of interfering intercalating metal species. For experimental convenience this study was performed in acetonitrile based liquid electrolytes. Measurements were performed as a function of whether the n-HfS_2 photoelectode was oriented perpendicular to the c-lattice vector ($\perp$-c), where a relatively defect-free van der Waals surface was exposed to the electrolyte, or parallel to the c-lattice vector ($\parallel$-c) where a high population of interstitial sites would be exposed to the non-aqueous electrolyte.

EXPERIMENTAL

Single crystals of n-HfS_2 were prepared by the halogen (I_2) vapor trans-

port technique (Northwestern University). Initial solid-state chemical reaction between Hf (99.5%) and S (99.999%) was accomplished by heating an intimate mixture together with 5mg I_2/ml of the quartz transport tube volume. This was performed in a three temperature zone furnace. Typical thermal gradients used were between 875°C and 800°C. Crystal growth occurred over 25 days. In all cases the relatively large crystals obtained were intrinsically n-type. Ohmic contact to n-HfS_2 was accomplished by sparking indium onto one side of the crystal using a 15 volt DC power supply. This was performed using a fine indium wire as a cathode with the other pole of the power supply clamped to the n-HfS_2 single crystal. When the indium wire was within ≈1mm of the crystal, a transient spark could be observed. This resulted in the ion implantation of indium into the ohmic contact region. Current collection was performed with a nichrome wire attached with silver epoxy and cured at 120°C for 1h. Photoelectrodes were then appropriately isolated from later contact with the electrolyte by epoxy (Norton Chemplast), so that only the single crystal front face of interest was exposed. Typical photoelectrode areas for ⊥-c oriented crystals was $0.04cm^2$ and $0.06cm^2$ for ∥-c surfaces.

Measurements were performed in a standard glass H-cell arrangement using a platinum counter electrode. SCE was used as a reference to the working electrode compartment via a salt bridge. Photoelectrode potentials were controlled by a Stonehard Associates BC 1200 potentiostat. Impedance, conductance and capacitance measurements were performed using a Hewlett-Packard 4276A digital LCZ meter over the frequency range 20kHz - 100Hz.

RESULTS AND DISCUSSION

Work performed was directed towards investigating the interfacial characteristics of single crystal n-HfS_2 as a function of crystal orientation in liquid non-aqueous electrolyte (acetonitrile containing 0.1M tetrabutylammonium fluorphosphate ($TBAPF_6$)) as the supporting electrolyte in the absence of potentially intercalating transition metal species. This investigation emphasizes the application of capacitance, impedance and admittance measurement techniques towards such a goal.

Mott-Schottky (MS) measurements were performed on the cell n-HfS_2/0.1M $TBAPF_6$,CH_3CN/Pt for both ⊥-c and ∥-c single crystal orientations over the frequency range 800Hz to 20kHz. Capacitance measurements at frequencies be- [illegible] 0kHz showed little dependency upon applied electrode potential

This indicated small changes in potential drop across the semiconductor depletion layer with the majority of applied potential being present in the electrolyte Helmholtz layer. At lower frequencies (800-1200Hz) MS data showed some frequency dependence as shown respectively in Figures 2 and 3 for ⊥-c and ∥-c oriented $n\text{-}HfS_2$ electrode. Table 1 summarizes flat band potential (V_{FB}) and carrier density (N_D) values obtained from the MS relationship at 1kHz as a function of crystal orientation. A dielectric constant of 5 was used in these calculations and assumed as a first approximation to be independent of surface orientation. In general, more negative V_{FB} and larger N_D values were obtained for the ∥-c oriented $n\text{-}HfS_2$ crystal face compared to the ⊥-c surface.

The observed frequency dependency of capacitance when lower measurement frequencies were used implied that the $n\text{-}HfS_2$/acetonitrile interfacial region could not be represented by a simple equivalent circuit model consisting of frequency independent capacitors and resistors. As a consequence, an equivalent circuit analysis model of this interface was performed using methodology previously discussed by others[29,30]. In this approach the liquid junction was represented by a continuous distribution of individual elements comprising series resistances and capacitances, resulting in a large number of relaxation times. These individual elements can originate from a variety of charge accumulation modes, such as surface states, inhomogeneous doping and surface crystal defects. For a large distribution of elements, the equivalent circuit could be represented by a frequency dependent resistor, R_v, in parallel with a frequency dependent capacitor, C_v, and a frequency independent capacitor C_{sc} representative of the space charge layer capacitance. The model may also incorporate electrolyte resistance and double layer capacitance, if appropriate. Expressions for the total admittance Y, impedance Z, conductance G, and susceptance B, for an equivalent circuit consisting of a large number of R-C elements, could be represented by the following relationships:

$$Y = a\omega^n + kb\omega^n \qquad (1)$$

$$Z = A\omega^{-n} - jB\omega^{-n} \qquad (2)$$

$$G = a\omega^n \qquad (3)$$

$$B = b\omega^n \qquad (4)$$

where A, B, a, b and n are characteristic circuit constants and ω is the angular frequency.

By use of such a model circuit, frequency dependent capacitance effects

at the n-HfS_2/electrolyte interface could be eliminated by extrapolating experimentally determined capacitance measurements to infinite frequency. The value of n required by the above capacitance measurements was obtained by determination of the cells frequency dependent conductance. In order to determine the equivalent circuit for the n-HfS_2/acetonitrile interface, capacitance, impedance and conductance responses were taken over the frequency range 20kHz - 100Hz at the dark photoelectrode. Figures 4 and 5 summarize respectively impedance and admittance responses for ⊥-c oriented n-HfS_2 at the two electrode potentials -0.022 and -0.172V vs. SCE. As can be seen, all of this data was linear and went through the origin. Thus, no influence by either the electrolyte resistance or double layer capacitance was evident. The equivalent circuit for the cell could therefore be represented by the space charge capacitance, C_{sc} at the n-HfS_2 surface being in-parallel to the frequency dependent components R_v and C_v[29,30], as shown in Figure 6a.

The impedance and admittance responses for ∥-c oriented n-HfS_2 in acetonitrile at -0.103 and -0.253V vs. SCE are summarized in Figures 7 and 8 respectively. Linear dependencies were found between real and imaginary parts of the measured cell impedance. Extrapolation to infinite frequency indicated cell electrolyte resistance to be 200Ω (Figure 7A). Similar electrolyte resistance values were obtained upon analysis of high frequency impedance data at -0.253V vs. SCE (Figure 7B). In this latter case however, impedance data obtained in the lower frequency region (below 6kHz) possesses a somewhat different slope. This may have reflected the presence of additional surface states other than those associated with exposed van der Waals layer edges at the semiconductor surface. The admittance responses shown in Figure 8 possessed radii between 2.3-2.5 x 10^{-3} 1/Ω, close to the reciprocal of the electrolyte resistance. The equivalent circuit used here for ∥-c oriented n-HfS_2 is shown in Figure 6b.

The high frequency region of the impedance/admittance response data was used to determine the n-HfS_2 space charge capacitance. The magnitude of C_{sc} was usually relatively small compared to C_v and in the low frequency range its contribution can often be neglected[33,34]. The relationship between log G and log ω, where G represents the total conductance of the cell corrected for electrolyte resistance, are summarized in Figure 9a-d for both ⊥-c and ∥-c oriented n-HfS_2. From the slopes obtained here the parameter characterizing

an exponential dependency between cell conductance and frequency, n, (eq. 3) could be obtained and used in extracting frequency independent capacitance at the semiconductor/electrolyte junction. As can be seen, n values were usually found between 0.7 and 0.8. An n value of 1 would have suggested the absence of frequency dependent capacitance effects at the n-HfS_2/electrolyte interface as implied from relationships 5 and 6[29,30]:

$$B = \omega C_V \quad (5)$$

$$C_V = b\omega^{n-1} \quad (6)$$

The frequency dependence of measured cell capacitance at two electrode potentials, are summarized in Figure 10 for both n-HfS_2 orientations. For ∥-c oriented n-HfS_2 in order to calculate capacitance, the cell susceptance value (B) was initially corrected for electrolyte resistance. Extrapolating the capacitance curves to infinite frequency eliminated the frequency dependent capacitance C_V, thereby permitting frequency independent capacitance values to be obtained. A comparison is made in Table 1 between capacitance data obtained at 1kHz and capacitance data obtained using the frequency-independent analysis of the electrode capacitance. It should be noted that from frequency independent data, capacitance values of 10^{-8}F/cm^2 (at E = -0.022V) were obtained from ⊥-c oriented n-HfS_2 which compares to an order of magnitude higher values (2.5×10^{-7}F/cm^2) for ∥-c oriented material (at E = -0.103V). Such differences may be attributed to a higher population of surface states for ∥-c oriented n-HfS_2. For high frequency measurements, many surface states will not be able to follow the applied AC voltage[35,36], whereas at lower frequencies the cumulative capacitance of both surface states and the van der Waals layers (∥-c) exposed to the electrolyte will be monitored.

The frequency independent capacitance values obtained above were used to plot frequency independent MS data (Figure 11). The number of charges on ∥-c oriented n-HfS_2 was found to be about three orders of magnitude higher than found on the van der Waals layer (Table 1). Such an observation supports previous results on d-band semiconductors, which suggested that accumulation of positive charges on surface states can occur at exposed ∥-c oriented layer type surfaces[12,23]. The presence of a high density of charged species in the proximity of such edge sites could in part explain the higher conductivity values found through rather than across the van der Waals layers[37]. The frequency independent MS data (Figure 11A) for ⊥-c oriented n-HfS_2 gave sim-

Table 1. Mott-Schottky parameters determiend for single crystal n-HfS_2 at ∥-c and ⊥-c orientations in CH_3CN containing 0.1M $TBAPF_6$.

⊥-c Oriented n-HfS_2 Photoanode, OCP +0.44V

	Mott-Schottky Relation, 1kHz	Frequency Independent Mott-Schottky Relation
C_{sc} (F/cm^2) at -0.022V	$6.1x10^{-8}$	$1x10^{-8}$
V_{FB} (V)	-0.40	-0.26
N_D ($\frac{1}{cm^3}$)	$5.3x10^{16}$	$3.4x10^{14}$

∥-c Oriented n-HfS_2 Photoanode, OCP -0.103V

	Mott-Schottky Relation, 1kHz	Frequency Independent Mott-Schottky Relation
C_{sc} (F/cm^2) at -0.103V	$1.1x10^{-6}$	$2.5x10^{-7}$
V_{FB} (V)	-0.80	-0.51
N_D ($\frac{1}{cm^3}$)	$1.3x10^{19}$	$7.1x10^{17}$

ilar V_{FB} values to that obtained at 1kHz (-0.4 vs. -0.26, Table 1). Differences between frequency independent MS and conventional MS data becomes greater for ∥-c oriented material, probably a consequence of the higher population of surface states on this latter orientation[38]. Energy level diagrams for ⊥-c and ∥-c oriented n-HfS_2 are shown respectively in Figure 12 and are based upon charge density and flat band potential data obtained for n-HfS_2 as determined from frequency independent MS data. A value of $2.5 \times 10^{19}cm^{-3}$ for the effective density of states in the conduction band was used in this calculation. The n-HfS_2 surface barrier for ⊥-c oriented material was found ≅0.4V and for ∥-c ≅0.3V. The consequent lower degree of band bending found for ∥-c oriented n-HfS_2 photoelectrodes was reflected in the generally lower photopotentials found for this material (80-160mV compared to 240-350mV for ⊥-c n-HfS_2 surfaces). The impedance and admittance responses obtained from both ⊥-c and ∥-c oriented n-HfS_2 indicated some instability at lower frequencies (usually below 800Hz), suggesting the possible presence of surface state related redox electrochemistry.

In order to detect surface states at both ⊥-c and ∥-c oriented n-HfS_2, together with comparing frequency independent impedance-admittance parameters with those obtained using more conventional MS measurement techniques, admittance spectroscopy analysis techniques were used[31,32].

In the simplest case the n-HfS_2/electrolyte interface was assumed to consist of the space charge capacitance, C_{sc}, connected in series with a bulk conductance G_{el}. By comparing real and imaginary parts of the admittance equation for such an equivalent circuit, with the appropriate in-phase admittance components being obtained experimentally, the following relationship can be obtained:

$$G/\omega = \frac{\omega\, C_{sc}^2\, G_{el}}{G_B^2 + (\omega C_{sc})^2} \tag{7}$$

where G represents the measured in-phase cell conductance. By plotting G/ω vs. ω a maximum will be given at

$$G/\omega_{max} = C_{sc}/2 \tag{8}$$

from which the space charge capacitance could be determined. If surface states are present on the n-HfS_2 surface, additional peaks will be observed possessing a different characteristic frequency ω'_{max} similar to relationship (8) above. Figure 13 compares plotting log G/ω vs. log ω for n-HfS_2 oriented both ⊥-c (curves A) and ∥-c (curves B). For ⊥-c oriented material no space charge

capacitance peak was evident at higher frequencies. A small value of C_{sc}, expected based upon previous impedance measurements (Figure 11 and Table 1), suggests that frequency maximum relating to charge accumulation might occur at frequencies above 20kHz[31,32]. The small peak observed at log $\omega \cong 4.1$ suggested the presence of surface state absorption effects. For ⊥-c oriented material, increasing G/ω values were observed at lower frequencies, indicating the presence of a Faradaic cell resistance component. Extrapolating log G/ω to zero ω indicated a Faradaic resistance of $10^7\Omega$ suggesting a high degree of polarizability and low exchange current densities at the n-HfS_2 electrode surface, as might be expected since no electroactive species were present in the non-aqueous electrolyte. For ‖-c oriented material (curves B) the high frequency peak observed was associated with the semiconductor space charge capacitance giving a value of $4.8 \times 10^{-7} F/cm^2$. In comparison a capacitance value of $2.5 \times 10^{-7} F/cm^2$ was obtained from frequency independent impedance studies. Since the population of electrolyte exposed van der Waal layers was probably subtley different between these two experiments, these two capacitance values are in relatively good agreement. The peak observed at log $\omega \cong 3.7$ was again probably associated with absorption processes at the van der Waals surfaces.

These frequency independent studies on n-HfS_2 indicated that capacitance for the ⊥-c surface was about an order of magnitude lower than that for the ‖-c surface. The high capacitance of ‖-c oriented n-HfS_2 electrode was explained by a high population of surface states accumulating about three orders of magnitude more charges than the ⊥-c face. Those surface states capable of intercalation act as effective recombination centers permitting only smaller photopotentials to be realized.

ACKNOWLEDGEMENT

This work was supported in part by the Office of Naval Research.

REFERENCES

1. H. Tributsch and J. C. Bennett, J. Electroanalyt. Chem., 81, 97 (1977).
2. H. Tributsch, Z. Naturforsch, 32a, 972 (1977).
3. H. Tributsch, Ber. Bunsenges, Phys. Chem., 81, 361 (1977).
4. H. Tributsch, Ber. Bunsenges, Phys. Chem., 82, 169 (1978).
5. H. Tributsch, J. Electrochem. Soc., 125, 1086 (1978).

6. J. Gobrecht, H. Gerischer and H. Tributsch, Ber. Bunsenges. Phys. Chem., 82, 1331 (1978).

7. J. Gobrecht, H. Gerischer and H. Tributsch, J. Electrochem. Soc., 125, 2085 (1978).

8. S. M. Ahmed and H. Gerischer, Electrochim. Acta., 24, 705 (1979).

9. H. Tributsch, Solar Energy Materials, 1, 705 (1979).

10. H. Tributsch, H. Gerischer, C. Clemen and E. Bucher, Ber. Bunsenges. Phys. Chem., 83, 655 (1979).

11. H. Tributsch, J. Electrochem. Soc., 128, 1261 (1981).

12. H. Tributsch, Structure and Bonding, 49, 127 (1982).

13. J. A. Wilson and A. D. Yoffe, Adv. Phys., 18, 193 (1969).

14. A. R. Beal, J. C. Knights, and W. Y. Liang, J. Phys. C. Solid State Phys., 5, 3531 (1972).

15. H. P. Hughes and W. Y. Liang, ibid., 10, 1079 (1977).

16. F. R. Shepherd and P. M. Williams, J. Phys. C. Solid State Phys., 7, 4416 (1974).

17. R. B. Murray, R. A. Bromley, and A. D. Yoffe, ibid., 5, 746 (1972).

18. L. F. Mattheiss, Phys. Rev., B8, 3719 (1973).

19. P. G. P. Ang and A. F. Sammells, J. Electrochem. Soc., 129, 233 (1982).

20. P. G. P. Ang, C. J. Liu, A. A. Rossignuolo, A. J. Tiller and A. F. Sammells, Measurement Techniques for Photoelectrochemical Solar Cells, Eds. W. L. Wallace, A. G. Nozik, S. K. Deb and R. H. Wilson, Proc. Electrochem. Soc., 697-703, 1982.

21. M. S. Whittingham, Science, 192, 1126 (1976).

22. H. Tributsch, Appl. Phys., 23, 61 (1980).

23. W. Kautek, H. Gerischer and H. Tributsch, Ber. Bunsenges. Phys. Chem., 83, 1000 (1979).

24. B. G. Yacobi, F. W. Boswell and J. M. Corbett, J. Phys. C. Solid State Phys., 12, 2189 (1979).

25. N. Chandra, J. K. Leland and A. J. Bard, J. Electrochem. Soc., 134, 76 (1987).

26. G. V. Subbor Rao and J. C. Tsang, Mater. Res. Bull., 9, 921 (1974).

27. M. S. Whittingham, U.S. Pat. 4,040,917 (1977).

28. A. R. Beal and W. Y. Liang, Phil. Mag., 27, 1397 (1973).

29. J. F. McCann, S. P. S. Badwal and J. Pezy, J. Electroanal. Chem., 118, 115 (1981).

30. J. F. McCann and S. P. S. Badwal, J. Electrochem. Soc., 129, 551 (1982).

31. Peter A. Smith, "Electrical Characterization of Polycrystalline and Photochemical Solar Cells," M. S. Thesis, Colorado State University, Ft. Collins, 1980.

32. J. Dubow and R. Krishnar, "Novel Concepts in Electrochemical Solar Cells," SERI Final Report, Contract No. XS-0-9272-1 (October, 1981).

33. S. P. S. Badwal and H. J. de Bruin, Phys. Status Solidi., A, 54, 261 (1979).

34. I. D. Raistrick, Chun Ho and R. A. Huggins, J. Electrochem. Soc., 123, 1469 (1976).

35. A. Goetzberger, E. Klansman and M. J. Schulz, CRC Int. Rev. Solid State Sci., 6, 1 (1976).

36. K. W. Frese, Jr. and S. R. Morrison, J. Electrochem. Soc., 126, 1235 (1979).

37. J. A. Wilson and D. A. Yoffe, Adv. Phys., 18, 193 (1969).

38. S. R. Morrison, Electrochemistry at Semiconductor and Oxidized Metal Electrodes, Plenum Press, New York, 1980.

FIGURE CAPTIONS

Figure 1. X20 photograph of single crystal n-HfS_2 grown by halogen vapor transport showing van der Waals layers available for the electrochemical intercalation of metal species.

Figure 2. Frequency dependence of Mott-Schottky relation for a n-HfS_2 electrode at ⊥-c orientation in 0.1M $TBAPF_6$ in CH_3CN.

Figure 3. Frequency dependence of Mott-Schottky relation for n-HfS_2 electrode at ‖-c orientation in 0.1M $TBAPF_6$ in CH_3CN.

Figure 4. Impedance responses for an n-HfS_2 electrode at ⊥-c orientation in contact with 0.1M $TBAPF_6$ in CH_3CN at -0.022V (A) and -0.172V (B) vs. SCE. Counter electrode Pt.

Figure 5. Admittance responses for ⊥-c oriented n-HfS_2 in CH_3CN/0.1M $TBAPF_6$ electrolyte at A) -0.022V and, B) -0.172V vs. SCE. Counter electrode Pt.

Figure 6. Equivalent circuits used in this work for rationalizing the cell n-HfS_2/CH_3CN/Pt as a function of crystal orientation.

Figure 7. Impedance responses for ‖-c oriented n-HfS_2 in CH_3CN (0.1M $TBAPF_6$) at A) -0.103V (OCP) and, B) -0.253V vs. SCE. Counter electrode Pt.

Figure 8. Admittance responses for ‖-c oriented n-HfS_2 electrode in CH_3CN (0.1M $TBAPF_6$) at A) -0.103V (OCP) and, B) -0.253V vs. SCE. Counter electrode Pt.

Figure 9. Conductance frequency response for n-HfS_2 in CH_3CN (0.1M $TBAPF_6$) A) ⊥-c orientation at -0.022V, and B) ⊥-c orientation at -0.172V, C) ‖-c orientation at -0.103V (OCP), and D) ‖-c orientation at -0.253V, all versus SCE.

Figure 10. Capacitance frequency dependence for the cell n-HfS_2/0.1M $TBAPF_6$, CH_3CN/Pt A) ⊥-c oriented n-HfS_2 at -0.022V and -0.172V, B) ‖-c oriented n-HfS_2 at -0.103V and -0.253V. SCE used as reference electrode.

Figure 11. Frequency independent Mott-Schottky plot for n-HfS_2 in CH_3CN (0.1M $TBAPF_6$) A) ⊥-c oriented, B) ‖-c oriented.

Figure 12. Energy schemes for n-HfS_2 electrode in 0.1M $TBAPF_6$/CH_3CN. Flat band potentials are based on frequency-independent results.

Figure 13. Frequency dependence of G/ω values for n-HfS_2 electrode in CH_3CN (0.1M $TBAPF_6$). A) ⊥-c oriented, B) ‖-c oriented. Electrode potential (vs. SCE) is shown next to the curves.

Figure 1. X20 photograph of single crystal n-HfS_2 grown by halogen vapor transport showing van der Waals layers available for the electrochemical intercalation of metal species.

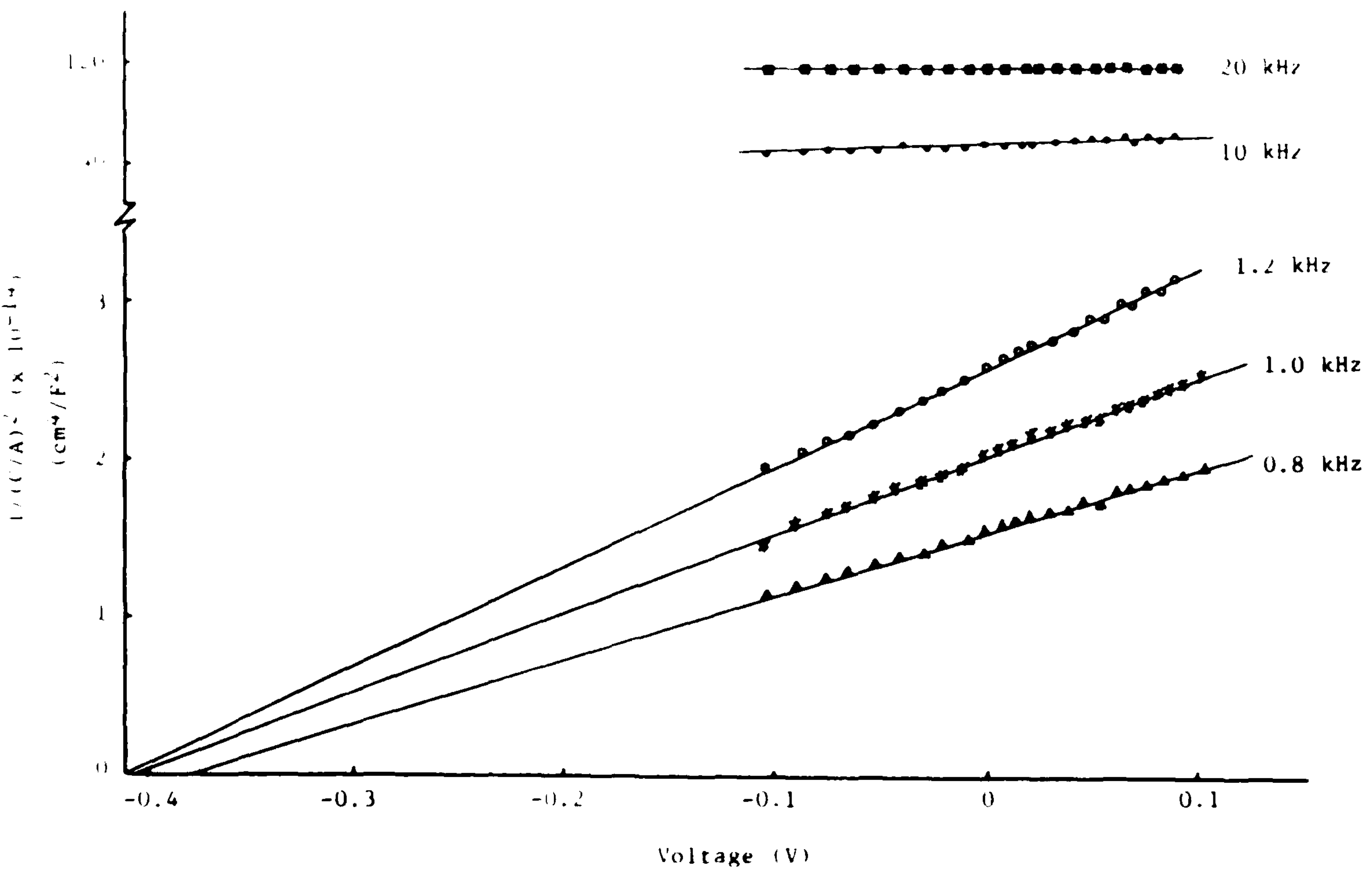

Figure 2. Frequency dependence of Mott-Schottky relation for a n-HFS_2 electrode at ⊥-c orientation in 0.1M $TBAPF_6$ in CH_3CN.

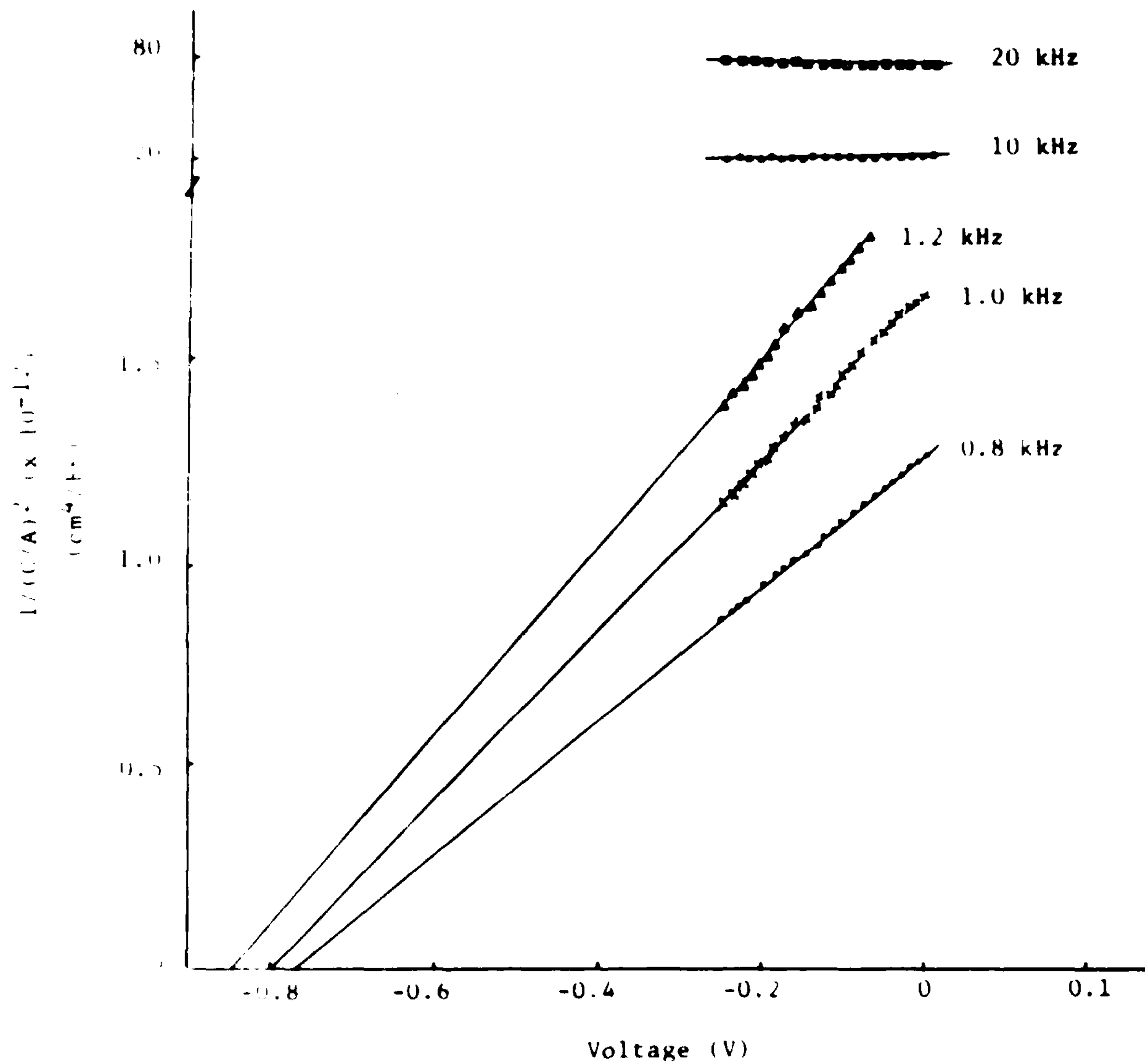

Figure 5. Frequency dependence of Mott-Schottky relation for n-HfS_2 electrode at ||-c orientation in 0.1M $TBAPF_6$ in CH_3CN.

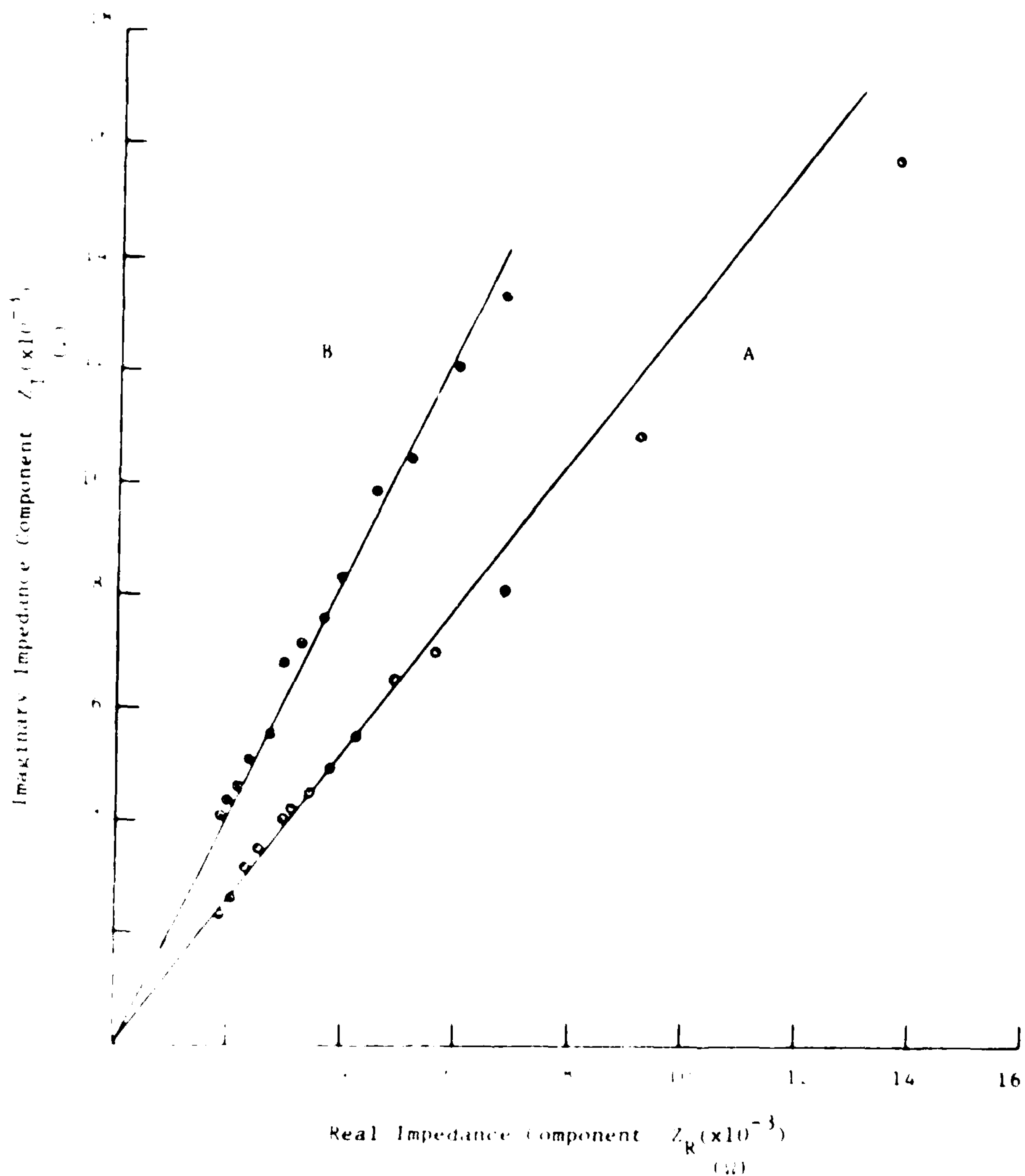

Figure 4. Impedance responses for an n-HfS$_2$ electrode at ⊥-c orientation in contact with 0.1M TBAPF$_6$ in CH$_3$CN at -0.022V (A) and -0.172V (B) vs SCE. Counter electrode, Pt.

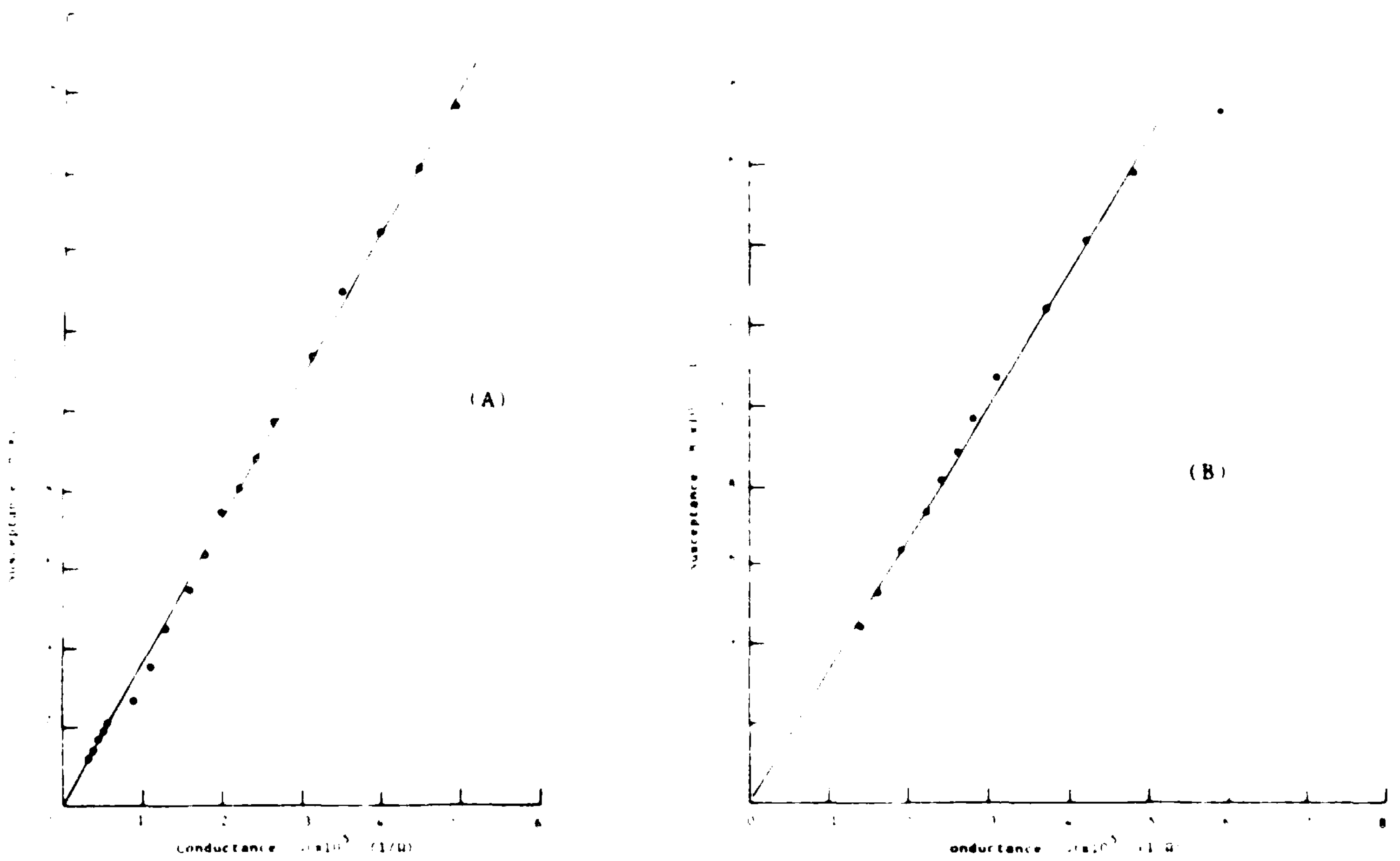

Figure 5. Admittance responses for $\perp$-c oriented n-HfS_2 in CH_3CN/0.1M $TBAPF_6$ electrolyte at A) -0.022V and, B) -0.172V vs. SCE. Counter electrode Pt.

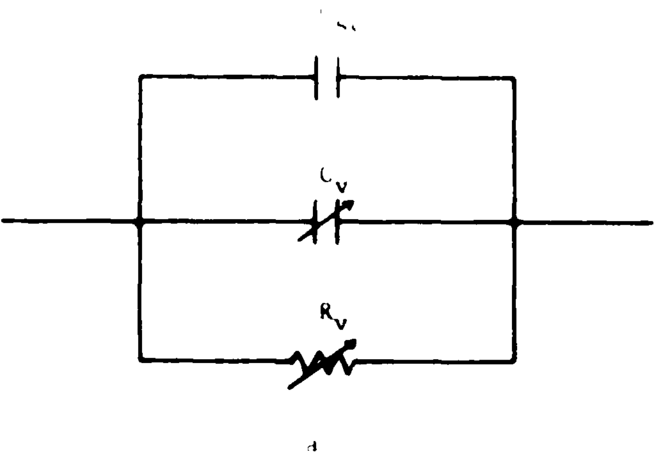

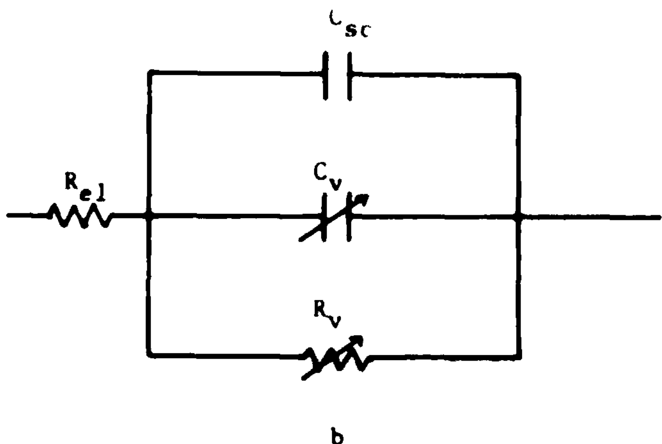

Figure 6. Equivalent circuits used in this work for rationalizing the cell n-HfS_2/CH_3CN/Pt as a function of crystal orientation.

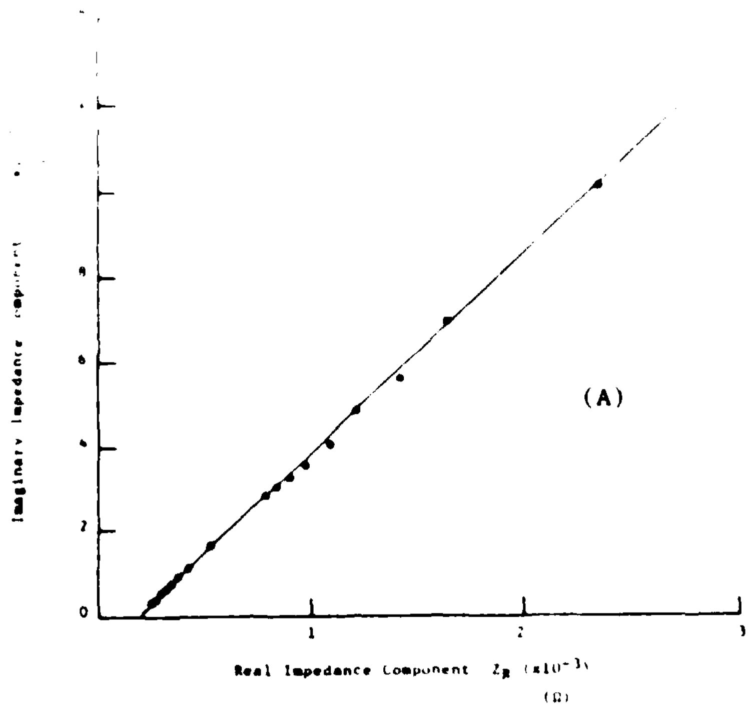

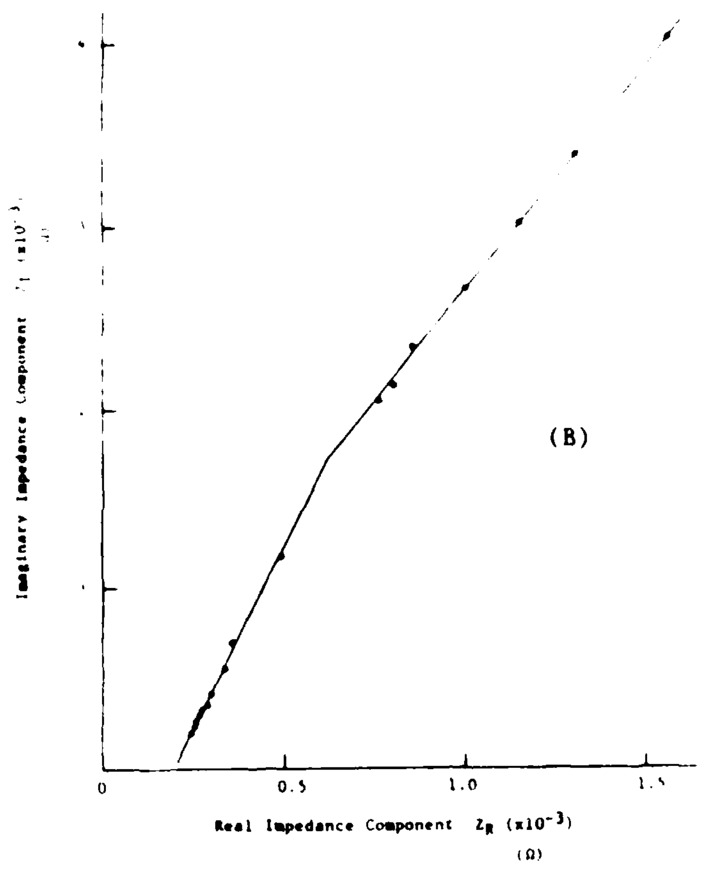

Figure 7. Impedance responses for ||-c oriented n-HfS_2 in CH_3CN(0.1M $TBAPF_6$) at A) -0.103V(OCP) and, B) -0.253V vs. SCE. Counter electrode Pt.

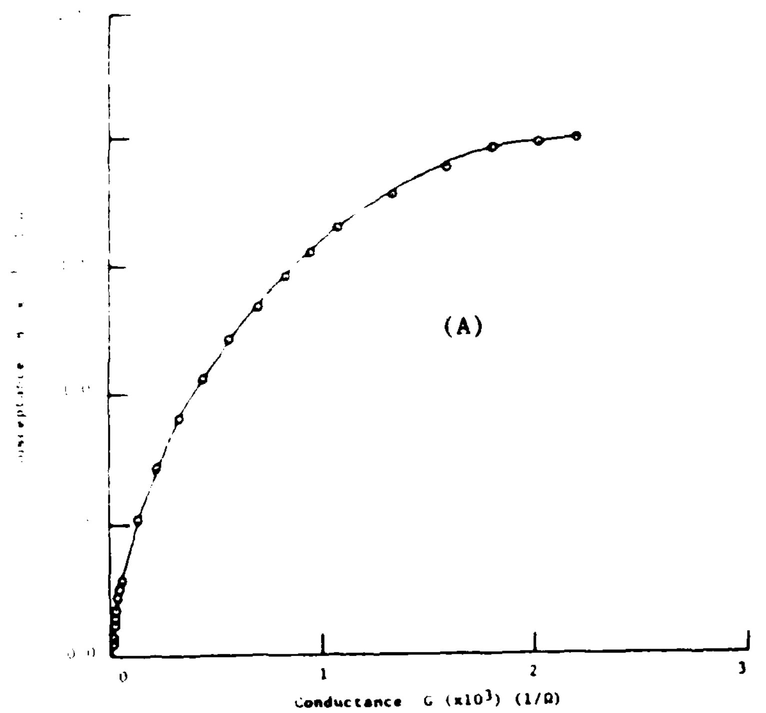

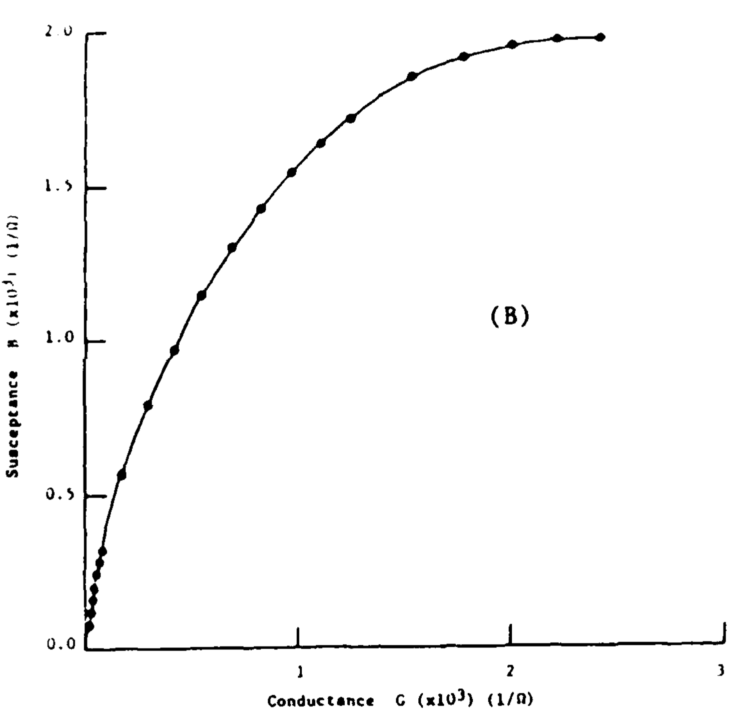

Figure 8. Admittance responses for ||-c oriented n-HfS_2 electrode in CH_3CN(0.1M $TBAPF_6$) at A) -0.103V(OCP) and, B) -0.253V vs. SCE. Counter electrode Pt.

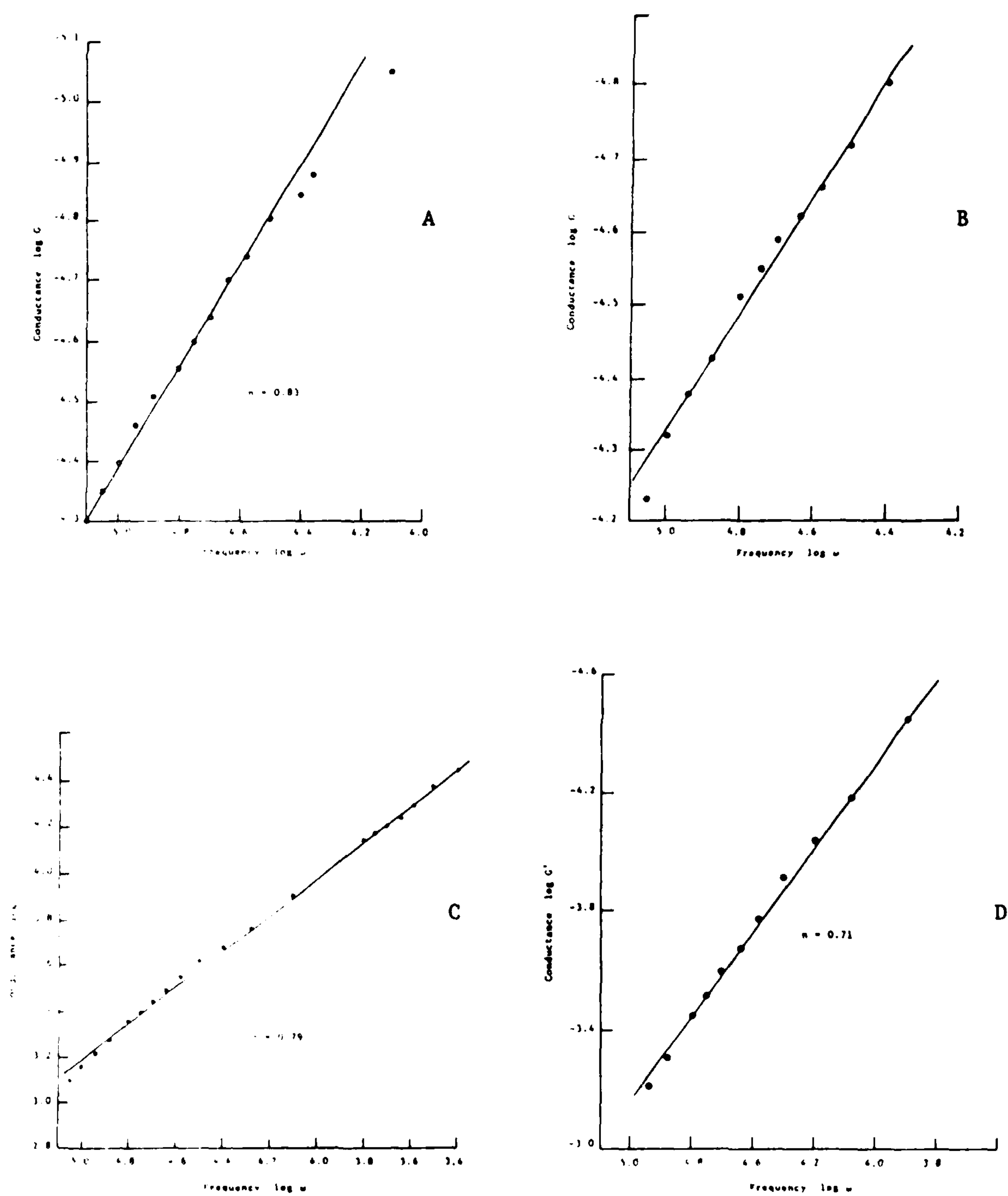

Figure 9. Conductance frequency response for n-HfS_2 in CH_3CN (0.1M $TBAPF_6$) A) ⊥-c orientation at -0.022V, and B) ⊥-c orientation at -0.172V; C) ∥-c orientation at -0.103V(OCP), and D) ∥-c orientation at -0.253V, all versus SCE.

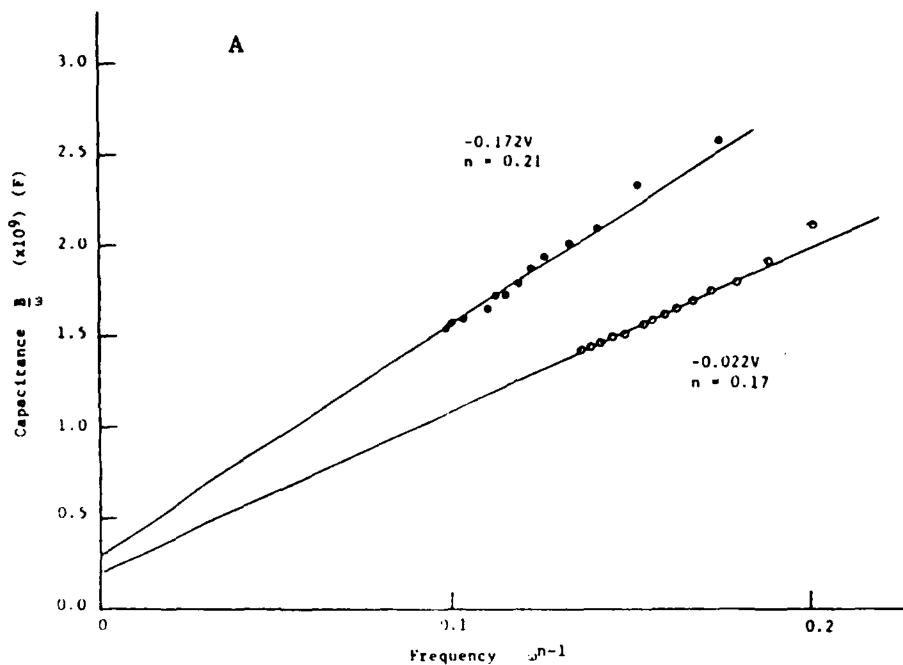

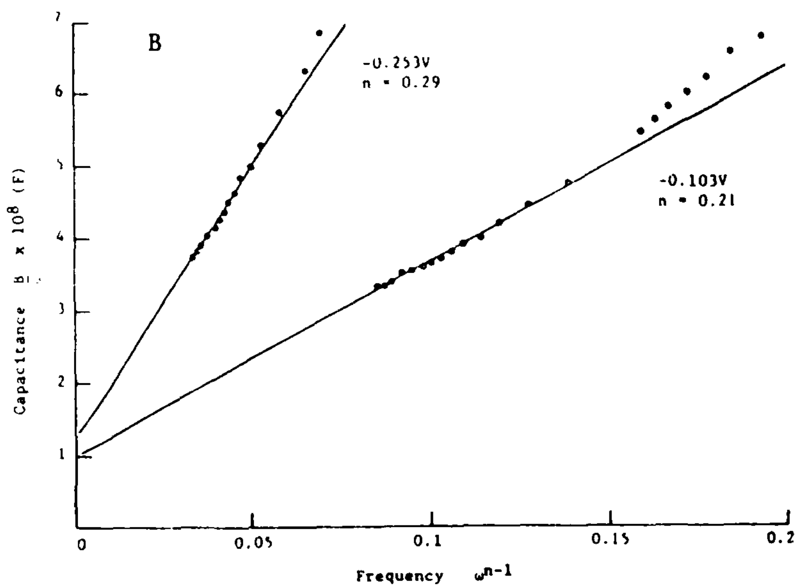

Figure 10. Capacitance frequency dependence for the cell n-HfS_2/ 0.1M $TBAPF_6$,CH_3CN/Pt A) ⊥-c oriented n-HfS_2 at -0.022V and -0.172V, B) ||-c oriented n-HfS_2 at -0.103V and -0.253V. SCE used as reference electrode.

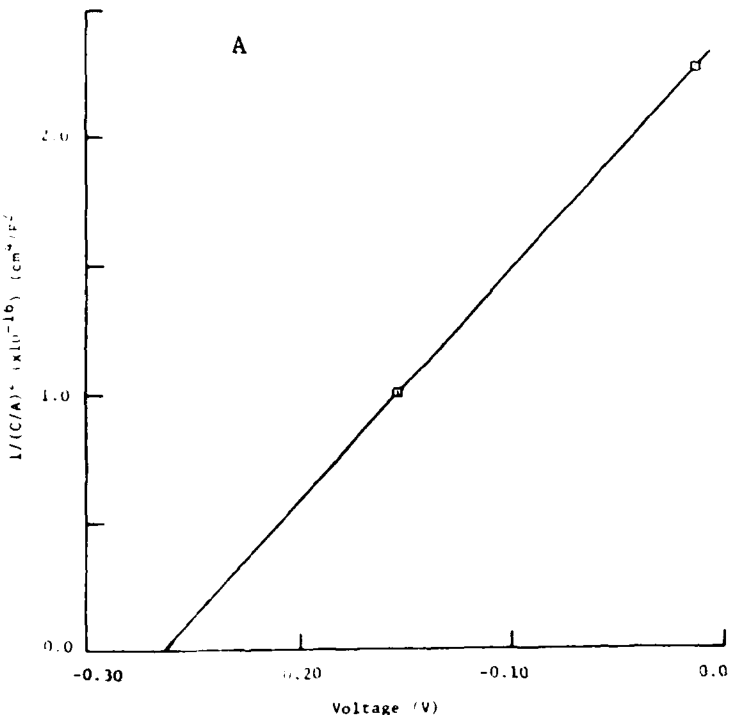

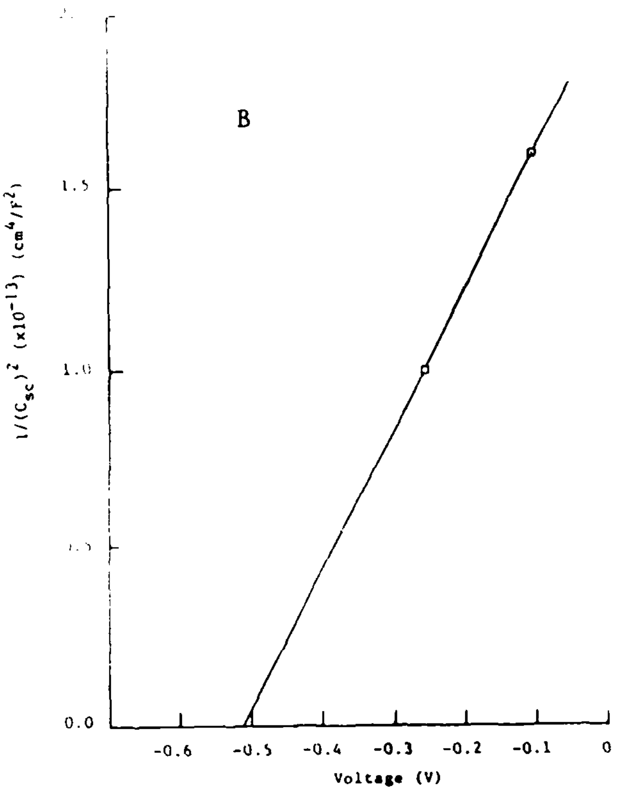

Figure 11. Frequency independent Mott-Schottky plot for n-HfS_2 in CH_3CN(0.1M $TBAPF_6$)
A) ⊥-c oriented, B) ∥-c oriented.

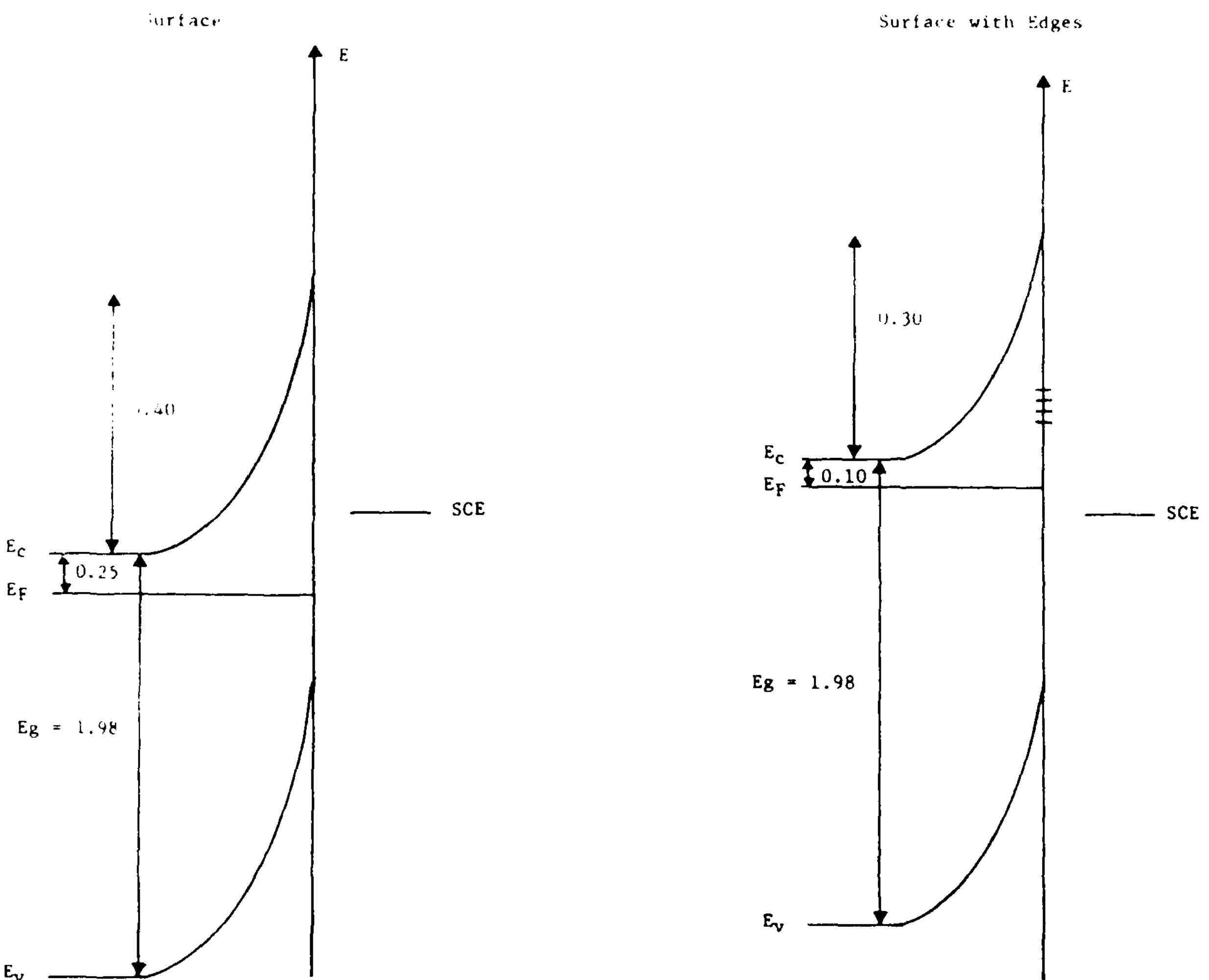

Figure 12. Energy schemes for n-HfS_2 electrode in 0.1M $TBAPF_6/CH_3CN$. Flat band potentials are based on frequency-independent results.

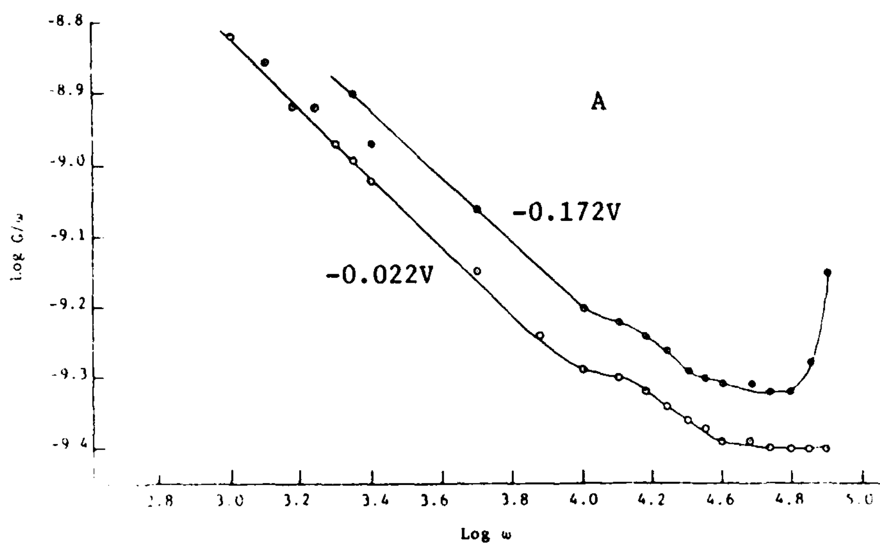

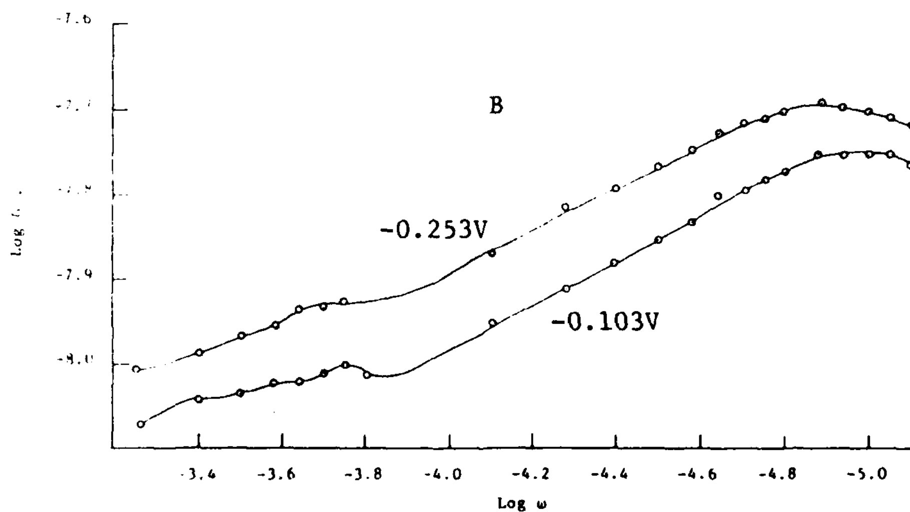

Figure 13. Frequency dependence of G/ω values for n-HfS_2 electrode in CH_3CN (0.1M $TBAPF_6$). A) $\perp$-c oriented, B) $\parallel$-c oriented. Electrode potential (vs. SCE) is shown next to the curves.

END
9-87
DTIC